NANO LETTERS

pubs.acs.org/NanoLett Letter

Direct Patterning of Perovskite Nanocrystals on Nanophotonic Cavities with Electrohydrodynamic Inkjet Printing

Theodore A. Cohen, David Sharp, Kyle T. Kluherz, Yueyang Chen, Christopher Munley, Rayne T. Anderson, Connor J. Swanson, James J. De Yoreo, Christine K. Luscombe, Arka Majumdar, Daniel R. Gamelin,* and J. Devin Mackenzie*

Cite This: https://doi.org/10.1021/acs.nanolett.2c00473 Read Online

ACCESS | Metrics & More | Article Recommendations | Supporting Information

ABSTRACT: Overcoming the challenges of patterning luminescent materials will unlock additive and more sustainable paths for the manufacturing of next-generation on-chip photonic devices. Electrohydrodynamic (EHD) inkjet printing is a promising method for deterministically placing emitters on these photonic devices. However, the use of this technique to pattern luminescent lead halide perovskite nanocrystals (NCs), notable for their defect tolerance and impressive optical and spin coherence properties, for integration with optoelectronic devices remains unexplored. In this work, we additively deposit nanoscale $CsPbBr_3$ NC features on photonic structures via EHD inkjet printing. We perform transmission electron microscopy of EHD inkjet printed NCs to demonstrate that the NCs' structural integrity is maintained throughout the printing process. Finally, NCs are deposited with sub-micrometer control on an array of parallel silicon nitride nanophotonic cavities and demonstrate cavity−emitter coupling via photoluminescence spectroscopy. These results demonstrate EHD inkjet printing as a scalable, precise method to pattern luminescent nanomaterials for photonic applications.

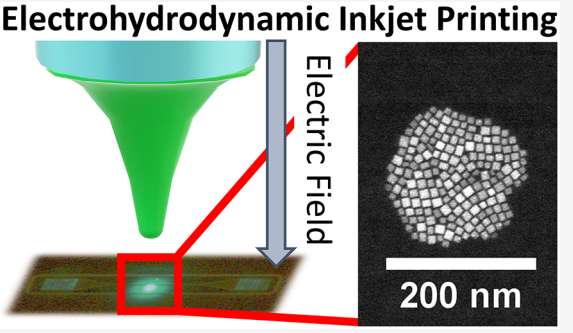

KEYWORDS: *perovskite nanocrystals, inkjet printing, photonic crystal cavity, transmission electron microscopy, additive manufacturing, hybrid integrated photonics*

Nanoscale patterning of materials has been critical for the rapid advancement of electronic information processing technologies.[1,2] The patterning of luminescent materials attracted early research interest,[3] and this capability has become critical for many emerging photonic device platforms where the precise heterointegration of emitters and other materials on nanophotonic structures is needed.[4,5] Inkjet printing has emerged as a promising method for patterning photoactive nanocrystals (NCs) because it is a rapid, mask-free method of placing on-demand droplets of a material into any arbitrary pattern with almost no material waste.[6−8] Typical inkjet printing resolutions are limited to tens of micrometers, which is less precise than is needed for integrated photonics. Smaller printed features can be generated with electrohydrodynamic (EHD) inkjet printing, a process that uses an electric field applied from the print nozzle to overcome surface energetics and viscous kinetics that limit mechanical droplet formation to generate droplets far smaller than those obtained with traditional inkjet printing.[9,10]

EHD inkjet printing of luminescent NCs has been used to manufacture light-emitting diodes,[11,12] photodetectors,[13] and chip-integrated plasmonic lasers.[14,15] Additionally, EHD inkjet printing has been investigated as a potential method for patterning luminescent materials on integrated photonic circuits because it is compatible with numerous substrate types and ink compositions. Early work in this area focused on integrating CdSe NCs with plasmonic structures,[16,17] and it was shown that in some cases, CdSe NCs could be placed on gold plasmonic wedge waveguides at the single-emitter level.[18] Organic dye molecules have also been coupled to photonic crystal cavities with EHD inkjet printing,[14] and a recent report demonstrated that quantum emitter behavior could be obtained from EHD inkjet printed terrylene dye molecules.[19] Since then, perovskite NCs have emerged as promising materials for quantum photonics due to their impressive lasing properties,[20,21] superior single-photon emission,[22,23] lifetime-limited excited-state spin coherence,[24] and intriguing collective emission properties.[25,26] These NCs have been patterned with subtractive optical lithography,[27−29] lower-resolution inkjet printing,[30,31] and EHD inkjet printing for LEDs[32] and radiative lifetime-encoded security tags,[33] but EHD inkjet printing has

Received: February 4, 2022
Revised: June 16, 2022

https://doi.org/10.1021/acs.nanolett.2c00473
Nano Lett. XXXX, XXX, XXX−XXX

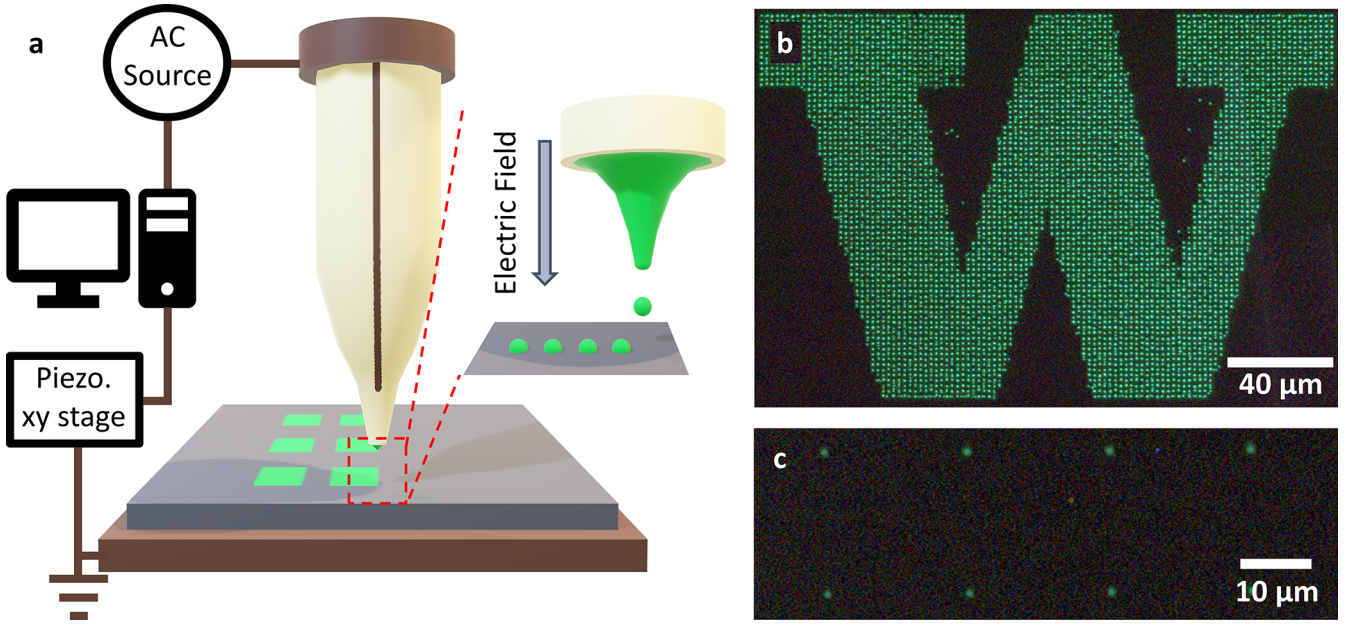

Figure 1. (a) Scheme describing the EHD inkjet printing setup. A computer-controlled AC source creates an alternating voltage profile between the print nozzle and the printer bed via a small electrode embedded in the print nozzle. This voltage generates an electric field between the print nozzle and the print substrate that drives printing. Inset: diagram showing the effect of an electric field on the meniscus at the tip of an EHD inkjet print nozzle. Partial polarization of the NC ink overcomes the ink's surface energy and draws a convex Taylor cone out of the EHD nozzle to produce small droplets that form the final print pattern. PL microscope images of printed $CsPbBr_3$ NCs on a fluorinated SAM-treated silicon substrate with (b) 2 μm feature spacing and (c) 20 μm feature spacing.

not been used to deterministically place perovskite NCs on nanophotonic cavities, an advancement that is necessary to develop next-generation chip-integrated quantum photonic devices. Furthermore, given the many documented structural instabilities of individual perovskite NCs[34] and self-assembled arrays of these NCs,[35] a thorough analysis of these materials after EHD inkjet printing is necessary to evaluate whether the high voltages used during processing are compatible with these notoriously unstable materials.

In this work, we use EHD inkjet printing to deterministically position $CsPbBr_3$ NCs on nanophotonic structures. Atomic force microscopy (AFM) images and photoluminescence (PL) studies of the printed NCs show that tunable NC features with diameters of 500 nm and heights of 50 nm could be reproducibly fabricated without compromising the NCs' PL properties. Additionally, we use silicon nitride membrane transmission electron microscopy (TEM) grids to collect the first-high resolution TEM images of EHD printed NCs to date. These images show that, in some cases, 200 nm printed features containing <200 individual NCs can be fabricated with EHD inkjet printing. Finally, we demonstrate that this printing method can be used to deterministically place these NCs onto silicon nitride nanobeam cavities[21,36] with NC emission being successfully coupled to the cavity modes. These results show that perovskite NCs can be effectively processed with EHD inkjet printing with high precision and at scale for photonic device integration.

$CsPbBr_3$ NCs were synthesized and the original ligands were replaced with didodecyldimethylammonium bromide according to methods reported previously.[34,37] This synthesis yields orthorhombic perovskite NCs with an average edge length of 9.7 ± 2.1 nm and narrow ~520 nm PL with a PL quantum yield of ~80% (see Figure S1 in the Supporting Information). The NCs were then dispersed in a 1:1 mixture of octane and hexadecane at a NC concentration of $\sim 10^{-7}$ M for the formulation of a stable EHD printing ink dispersion. Figure 1a shows a schematic of the EHD inkjet printing setup used in this work. Printing is performed by applying a voltage between the electrode within the print nozzle and the substrate ground plane. This voltage polarizes the printing solution, creating an electric field that overcomes the intrinsic surface energy controlling the meniscus curvature of the EHD ink at the nozzle orifice, i.e. creating a Taylor cone at the tip of the print nozzle, as illustrated in the inset of Figure 1a. Computer control of the voltage parameters associated with this electric field allows droplet formation and acceleration toward the substrate, and the controlled movement of the substrate stage enables the printing of very high resolution patterns. Silicon and glass substrates coated with a fluorinated self-assembled monolayer (SAM) were used to prevent droplet spreading that could increase printed feature sizes. Printing was performed with "bump mode" waveform control, a method of printing where the control software stops the print nozzle at discrete points and applies a 75% square-wave AC potential with a frequency of 1 kHz, an amplitude of 200 V, and a bias of 400 V for a set time to dispense femtoliter-scale NC ink droplets at each point (see Figure S2 in the Supporting Information). This approach allows fine and arbitrary tuning of the NC drop spacing in any desired pattern.

Figure 1b,c shows PL microscope images of EHD inkjet printed $CsPbBr_3$ NCs under 450 nm excitation. The 210 μm print pattern in Figure 1b consists of 2 μm spaced NC features printed with a 70 ms hold time. Figure 1c shows a section of a 500 μm pattern composed of 20 μm spaced features printed with a 40 ms hold time. The hold times were selected on the basis of an optimization to maximize the ratio of on-target to off-target printed features, as exemplified in Figure S3 in the Supporting Information. Green PL is observed from each

https://doi.org/10.1021/acs.nanolett.2c00473
Nano Lett. XXXX, XXX, XXX−XXX

printed NC feature, and the 2 and 20 μm grid patterns are well maintained across the entire printed pattern with few defects. To test whether EHD inkjet printing affects the optoelectronic properties of the $CsPbBr_3$ NCs, steady-state PL studies of NCs before and after printing were conducted. Figure 2a shows PL

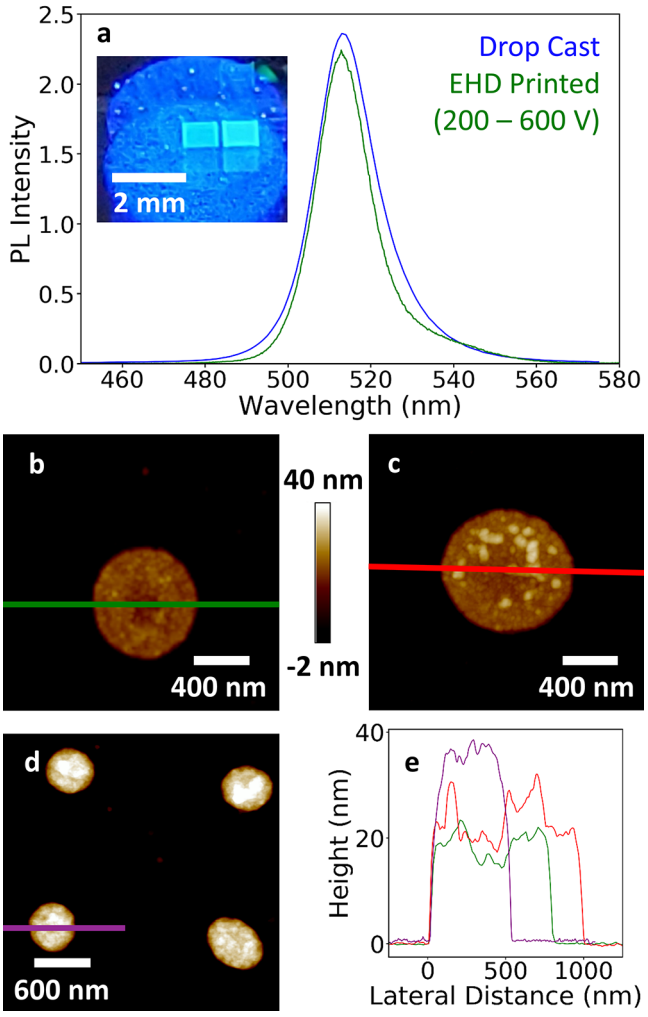

Figure 2. (a) Normalized PL spectra of $CsPbBr_3$ NCs drop-cast from hexanes solvent and EHD inkjet printed on a silicon substrate. Inset: photograph of printed patterns on a glass substrate, under 450 nm illumination. The 1 mm^2 print patterns visible here have different brightnesses because they were printed with different parameters and different numbers of print passes. AFM images of NCs printed with 20 μm feature spacing and bump hold times of (b) 40 ms and (c) 70 ms. (d) AFM image of NCs printed with 2 μm feature spacing. (e) Height profiles from the color-coded lines in the AFM images in panels (b)−(d) showing controllable, sub-micrometer NC feature sizes.

spectra of a printed NC feature and an ensemble of the same NCs drop-cast onto a silicon substrate. The PL spectrum of this large, printed feature is unchanged, but a minor blue shift is noted for smaller printed features (see Figure S4 in the Supporting Information). Furthermore, the inset of Figure 2a shows that, when NC print patterns are excited with 450 nm light, visible NC PL can be observed with the eye and imaged with a cell phone camera. The NCs thus remain bright following the EHD inkjet printing process.

Figure 2b−d shows AFM images of EHD inkjet printed $CsPbBr_3$ NCs, and Figure 2e shows height profiles collected along the color-coded lines shown in Figure 2b−d. These printed features are less than 1 μm in diameter, which highlights the high-resolution patterning capability of EHD inkjet printing. Figure 2d and the additional AFM image in Figure S5 show that remarkably consistent feature spacings of 2 μm can be readily achieved with this technique. The height profiles in Figure 2e further demonstrate that printed features can be reduced to diameters as small as 500 nm by optimizing print parameters. These liquid-ink-derived features show minimal "coffee ring" character and smaller final NC feature dimensions in comparison to features printed on untreated substrates. This indicates that the fluorinated SAM-coated silicon substrates result in a low liquid/solid interfacial energy even for this ink that is formulated with nonpolar solvents which tend to have low liquid/air interfacial energies and this surface that has a low solid/air interfacial energy.[38−40] This contributes to a dewetting effect that yields high-resolution print features and less evidence of liquid/solid contact line pinning. Additionally, while 500 nm diameter on-target features could be reproducibly formed, a further AFM analysis shown in Figure S5 in the Supporting Information shows that some off-target droplets form features with diameters below 300 nm, which suggests that further optimization of print parameters could yield even smaller on-target EHD printed NC features. Finally, the step heights observed for the prints shown here are all multiples of the NC edge length of ∼10 nm, demonstrating that these print features are likely composed of only two to four layers of $CsPbBr_3$ NCs.

Ideally, the NC crystal phase, size distribution, and cubic shape would all be preserved after printing. These characteristics can be measured by TEM, but EHD inkjet printed NCs have not been characterized with high-resolution TEM to date. The few reported TEM images of EHD printed structures were collected from silica structures on copper TEM grids generated with print biases between 6 and 12 kV[41,42] or from gold nanostructures printed on molybdenum half-grids for STEM imaging.[43] The voltages used for silica printing would likely be too high to adequately preserve perovskite NC PL properties, as discussed above, and we were unable to successfully print $CsPbBr_3$ NCs onto carbon-coated copper or nickel TEM grids at lower voltages due to the grids' high conductivity. Furthermore, the molybdenum half-grid approach cannot be used to collect high-resolution images or electron diffraction (ED) patterns of printed structures, which are important for assessing NC morphological and structural properties after printing. Therefore, we used carbon-coated Si_3N_4 membrane TEM grids to image our EHD inkjet printed NCs. Figure 3a,b shows optical microscope images of $CsPbBr_3$ NCs on collected in PL and dark field modes, respectively. Printing voltages (200−600 V) similar to those employed in Figures 1 and 2 were used to print on Si_3N_4 membrane TEM grids, and NC PL is clearly visible in regions both above the Si_3N_4 window and on the surrounding silicon support. We did not apply the same fluorinated SAM treatment to the Si_3N_4 TEM grids as was used on the silicon substrates discussed previously, which results in the printing of larger droplets in Figure 3a,b due to the surface energy differences between the carbon-coated TEM grids and the fluorinated SAM treated silicon substrates.[40] Nevertheless, the high-angle annular dark field scanning transmission electron microscope (HAADF-STEM) images in Figure 3c,d show that each printed feature comprises

https://doi.org/10.1021/acs.nanolett.2c00473
Nano Lett. XXXX, XXX, XXX−XXX

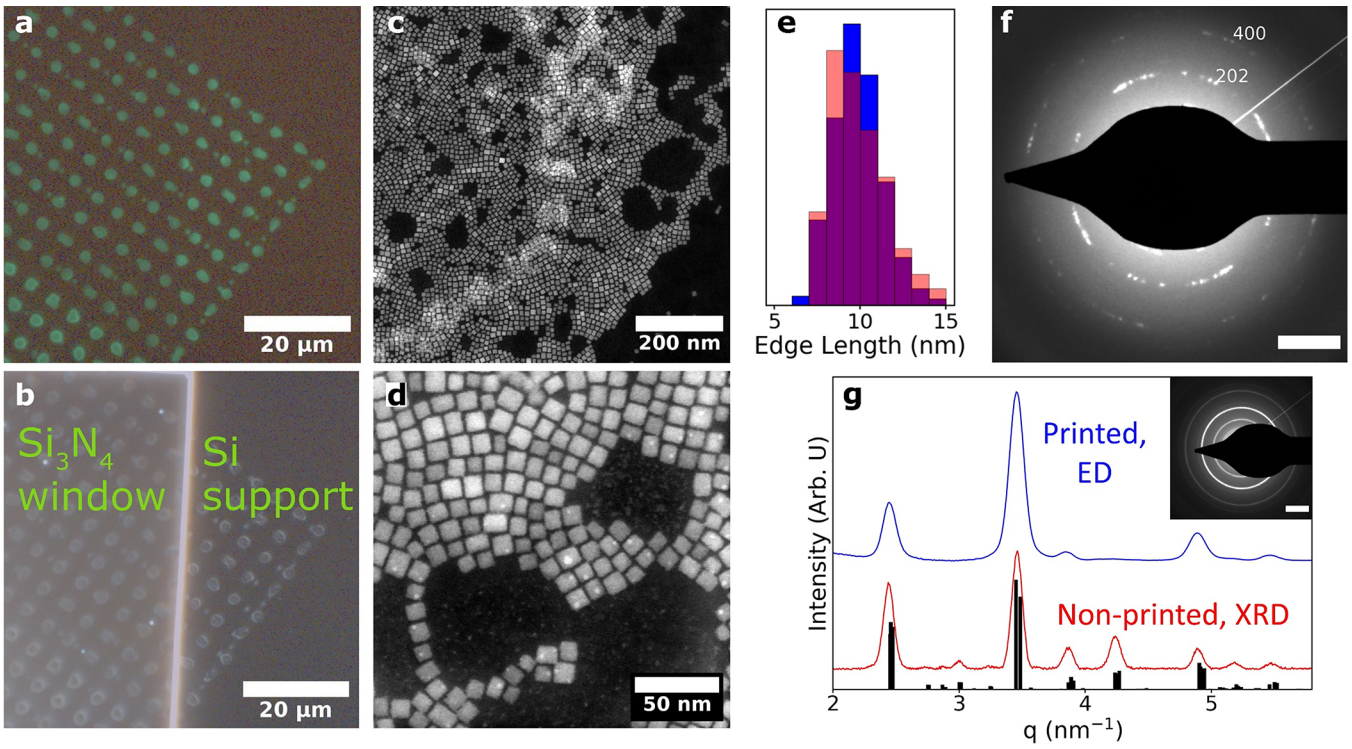

Figure 3. (a) PL microscope image of EHD inkjet printed $CsPbBr_3$ NCs on a carbon-coated Si_3N_4 membrane window TEM grid under 450 nm irradiation. (b) Dark field optical microscope image of the same area shown in (a). The bright white line is the edge of the Si_3N_4 TEM window. (c, d) HAADF-STEM images of $CsPbBr_3$ NCs within an EHD inkjet printed droplet. (e) Edge length distribution of EHD inkjet printed NCs (blue) and nonprinted NCs (red). (f) ED image of a selected area showing a spot diffraction pattern which indexes to the $CsPbBr_3$ *Pnma* lattice planes. (g) ED pattern ring integration of printed $CsPbBr_3$ NCs (blue) in comparison with the XRD pattern of nonprinted NCs (red) and a standard reference (black). The differing peak intensities are attributed to differences in preferential NC orientation in preparation for XRD and ED analysis. Inset: large-area ED image used to acquire the integrated pattern in (g). Scale bars in (f) and (g) are 2 nm^{-1}.

clusters of individually resolvable $CsPbBr_3$ NCs. Additionally, ordered NC superlattice domains are visible in these and the other printed NC STEM images shown in Figure S6 in the Supporting Information. We also find that some off-target printed features are as small as ∼200 nm in diameter and are composed of ≲200 individual nanocrystals (see Figure S7 in the Supporting Information). Figure 3e shows edge length distributions from NCs printed on Si_3N_4 TEM grids and drop-cast from hexanes onto a carbon-coated copper TEM grid. The average NC edge lengths before and after printing are 9.7 ± 2.1 and 9.8 ± 1.6 nm, respectively, which demonstrates that the NC size distribution is largely unchanged by the EHD inkjet printing process. NCs printed on TEM grids with printing biases between 250 and 1750 V have average edge lengths of 9.6 ± 1.8 nm (see Figure S7 in the Supporting Information). Figure 3f shows the ED obtained from a small area of the EHD inkjet printed NCs. The spot patterns in this image index to the orthorhombic $CsPbBr_3$ crystal lattice, and the alignment of the diffraction spots reinforces the observation that the printed NCs form self-assembled superlattice domains under these printing conditions. Finally, the radially integrated, large-area ED pattern in Figure 3g can be directly indexed to the orthorhombic $CsPbBr_3$ powder X-ray diffraction (XRD) reference pattern and the XRD data obtained for nonprinted $CsPbBr_3$ NCs, with no additional detectable crystal phases. Notably, the ED peak intensities differ from the powder XRD intensities, reflecting the preferred orientation of the printed NCs.

The patterns analyzed above were all printed on blank silicon substrates. To print NCs onto prefabricated Si_3N_4 nanobeam cavities,[36,44] we used an EHD inkjet printing alignment process to ensure that printed droplets were placed directly on the centers of the nanobeam cavities, as described in Figure S8 in the Supporting Information. Aligned print patterns were then coated with poly(methyl methacrylate) (PMMA) to encapsulate the NCs against environmental degradation during optical characterization and to preserve the inversion symmetry of the refractive index surrounding the cavity without affecting the NC PL (see Figure S9 in the Supporting Information). The nanobeam cavities are designed to maintain a high quality factor even when they are encapsulated in a polymer.[45] Figure 4a shows a PL microscope image of EHD inkjet printed NCs on a large array of nanobeam cavities. The inset of Figure 4b shows a magnified image of one individual nanobeam cavity, with additional images being given in Figure S10 in the Supporting Information. The green emission of the printed $CsPbBr_3$ NCs is clearly visible at the centers and at the grating couplers found at both ends of each nanobeam cavity waveguide. This result shows that the printed NC emission is successfully coupled into the nanobeam cavity and that EHD inkjet printing successfully placed NCs onto all the devices. Figure 4b shows the spectrum of emission emanating from the grating coupler of the nanobeam cavity in the inset of Figure 4b. In addition to the broad background PL of non-cavity-coupled NCs, a sharp peak at ∼517 nm is observed. This peak can be assigned to NC emission that is coupled to the cavity mode of

https://doi.org/10.1021/acs.nanolett.2c00473
Nano Lett. XXXX, XXX, XXX−XXX

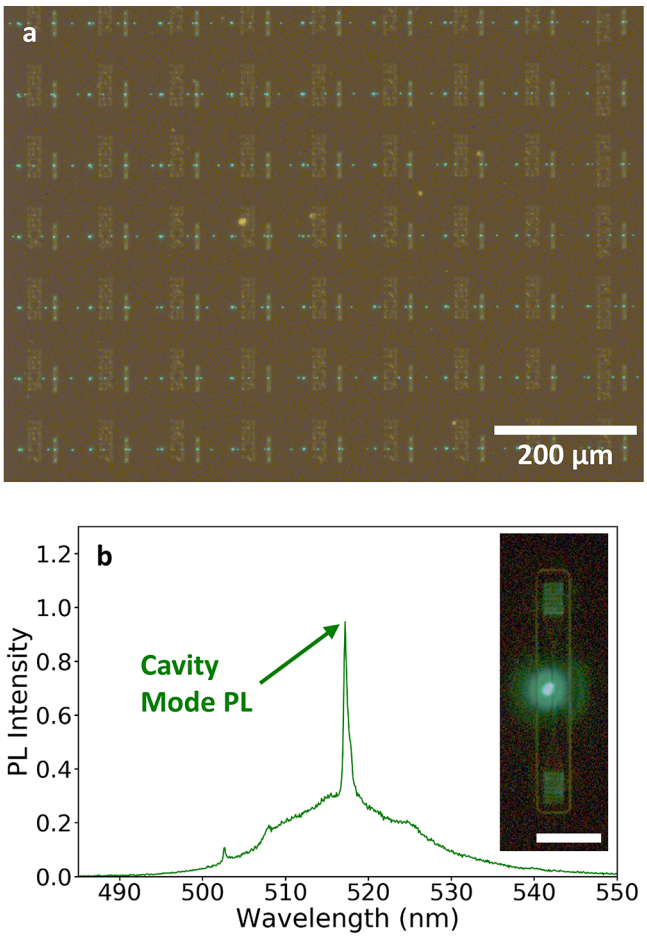

Figure 4. (a) PL microscope image of EHD inkjet printed $CsPbBr_3$ NCs on an array of prefabricated monolithic Si_3N_4 nanobeam cavities. NC features were printed with 50 μm spacing, and several off-target features are present. Visible PL can be seen emanating from the grating couplers at the top and bottom of each cavity. (b) PL spectra collected through a nanobeam cavity grating coupler. In addition to broad background $CsPbBr_3$ NC emission, a sharp peak is observed at ~517 nm, associated with NC PL coupled to the nanobeam cavity mode ($Q \approx 1000$). Inset: PL microscope image of the nanobeam cavity characterized in (b). The scale bar is 10 μm.

this nanobeam cavity. Lorentzian fitting of this peak reveals a Q factor of ~1000 for this cavity-coupled emission, which is in good agreement with the expected Q factors for this nanobeam cavity structure.[36] We also note an additional higher order cavity peak at ~503 nm. We attribute this mode to slight out-of-plane inversion symmetry breaking of the refractive index by the printed NCs.[44]

There are several important advancements in this work that demonstrate the potential of EHD inkjet printing for the integration of perovskite NCs with photonic devices. First, despite the promising structural characterization in prior reports of EHD inkjet printed CdSe[11,16] or perovskite[16,17] NCs, the TEM data presented here provide unique and comprehensive evidence of NC structure preservation and self-assembly during the printing process. This result is particularly important for perovskites because of their well-documented environmental instability and the potential of both single-perovskite NCs as single-photon sources[22,23] and self-assembled superlattices as superfluorescent correlated photon sources[25,26] for chip-integrated quantum photonics. We also collected TEM images of ~200 nm diameter off-target printed features that contain $\lesssim$200 individually resolvable NCs, which shows that this processing method can be used to place small, ordered arrays of perovskite NCs on substrates for quantum photonic device integration. The position of the printed NC PL maximum varies slightly after EHD inkjet printing, but the variations in peak position and spectral shape are minor. More spectral information is needed to precisely assign the origins of these variations, but we tentatively attribute the slightly blue shifted emission of small, printed features to reduced reabsorption.[46] Some irreversible etching of the NCs under these excitation conditions may further shift the PL maximum of these small, printed features to slightly higher energy in comparison to the lowest energy excitonic absorption feature of the original, nonetched NCs, but this etching can be mitigated with air-free measurements.[34] These samples did not generate sufficient PL intensity for PL quantum yield measurements. In some instances, microscope-integrated cavity measurements were used to successfully obtain this parameter for organic dyes.[47,48] Finally, while CdSe NCs have been EHD inkjet printed on plasmonic devices with near-micrometer precision,[17,18] and reports of EHD printed perovskite NCs demonstrate ink coalignment with a precision of ~10 μm,[33] this report demonstrates sufficient feature alignment precision to place perovskites on a ~10 mm^2 array of dielectric photonic crystal cavities with unmatched, sub-micrometer precision. The coalignment imprecision here is greater than one micrometer but can be improved by using a more precise print stage and alignment setup. Similarly, the Q factor of ~1000 demonstrated here can be improved through an improved cavity design.[21]

In summary, we have shown that $CsPbBr_3$ NCs can be deterministically patterned over large areas and with sub-micrometer precision using EHD inkjet printing. Additionally, we collected the first high-resolution STEM images of EHD inkjet printed structures, showing that the original NC structure is preserved post printing, that NCs within these printed structures self-assemble into superlattice domains, and that ~200 nm diameter printed features containing $\lesssim$200 NCs can be produced with this technique. We also used micrometer-scale alignment to place printed NC droplets onto the centers of a ~10 mm^2 array of prefabricated Si_3N_4 nanobeam cavities. This demonstration should motivate the further exploration of this printing method to process perovskite NCs for photonic devices, with the potential to leverage quantum emission from single printed perovskite NCs or self-assembled NC superlattices with monolayer thickness control. It should also motivate the exploration of EHD inkjet printing of other novel luminescent materials for photonic device integration.

EXPERIMENTAL PROCEDURES

Materials. Lead acetate trihydrate ($Pb(OAc)_2 \cdot 3H_2O$; 99.9%, Baker Chemical), cesium carbonate (Cs_2CO_3; 99.9%, Sigma-Aldrich), bromotrimethylsilane (TMS-Br; 97%, Sigma-Aldrich), 1-octadecene (ODE; 90%, Sigma-Aldrich), oleylamine (OAm; 70%, Sigma-Aldrich), oleic acid (OA; 90%, Sigma-Aldrich), didodecyldimethylammonium bromide (DDABr; 98%, Sigma-Aldrich), hexanes (99%, mixture of isomers, Sigma-Aldrich), ethyl acetate (99%, Sigma-Aldrich), toluene (HPLC, Fischer Chemical), octane (99%, Sigma-Aldrich), hexadecane (99%, Sigma-Aldrich), nitric acid (20%, EMD), trichloro(1*H*,1*H*,2*H*,2*H*-perfluorooctyl)silane (97%,

https://doi.org/10.1021/acs.nanolett.2c00473
Nano Lett. XXXX, XXX, XXX−XXX

Sigma-Aldrich), anisole (99.7%, Sigma-Aldrich), and poly(methyl methacrylate) (PMMA; M_w ~120000, Sigma-Aldrich) were used as received unless otherwise noted.

Nanocrystal Synthesis and Solution Preparation. $CsPbBr_3$ NCs were synthesized according to methods reported previously.[37] Once they were purified, the NCs were treated with DDABr according to methods reported previously.[34] Briefly, 600 μL of stock NC solution in hexanes was combined with 600 μL of toluene, 160 μL of a 0.05 M DDABr solution in toluene, and 30 μL of oleic acid in an N_2-filled glovebox. The resulting NCs were precipitated with ethyl acetate in air and centrifuged at 16060*g* for 10 min. The precipitated NCs were resuspended in hexanes and stored in an N_2-filled glovebox for future use. NC inks were prepared by removing a 100 μL aliquot of a hexanes NC solution from the glovebox and drying the NCs under N_2 flow. Once the NCs were dried, 500 μL portions of octane and hexadecane were added, and the resulting solution was filtered through a 220 nm PTFE syringe filter to yield a solution with a NC concentration of ~10^{-7} M. Hexadecane was chosen for its high boiling point to prevent drying and nozzle clogging during the printing process, but additional octane was necessary to facilitate the suspension of these NCs in solution. All NC inks were used within 1 day of preparation. PMMA solutions were prepared by stirring 80 mg mL^{-1} of PMMA in anisole overnight and filtering through a 460 nm PTFE syringe filter.

Electrohydrodynamic Inkjet Printing. Printing was performed with an SIJ Technologies S050 EHD inkjet printer. Substrates were cleaned with concentrated nitric acid overnight and washed with DI water. Clean substrates were then coated with a low-surface-energy fluorinated SAM by placing the substrate on a 160 °C hot plate under a Petri dish with 10 μL of trichloro(1*H*,1*H*,2*H*,2*H*-perfluorooctyl)silane for 1 h prior to mounting on the EHD inkjet printer stage. A fresh superfine EHD inkjet print nozzle with an ~2 μm inner diameter was then loaded with 10 μL of NC ink using a custom-designed narrow pipet tip, and the print nozzle was magnetically mounted to the EHD inkjet printer. The nozzle tip was lowered to ~10 μm above the substrate, and printing was performed in bump mode with a 75% square waveform between 200 and 600 V operating at a frequency of 1 kHz unless otherwise noted. The bed speed and bump hold time were tuned to the desired droplet spacing and print consistency (see Figure S3 in the Supporting Information). To print droplets aligned to prefabricated device substrates, E-beam etched marks on the device substrate were found with the printer's built-in alignment camera, and the associated stage location was saved in the software. A nozzle alignment mark was then printed on the substrate and found with the alignment camera, and the associated alignment camera location was saved in the software. This information, along with the spacing between nanobeam cavity devices on the substrate, was used to calibrate the coordinate plane of the stage and the alignment camera to the movement of the nozzle, thereby enabling the placement of NC droplets onto the center of Si_3N_4 nanobeam cavities with micrometer-scale precision (see Figure S8 in the Supporting Information). If necessary, 100 μL of PMMA solution in anisole was spin-coated onto the printed substrate at 2000 rpm for 1 min. The substrate was then annealed at 70 °C for 10 min.

■ ASSOCIATED CONTENT

Supporting Information

The Supporting Information is available free of charge at https://pubs.acs.org/doi/10.1021/acs.nanolett.2c00473.

Spectroscopic experimental procedures, print parameter optimization, and additional printed NC characterization (PDF)

■ AUTHOR INFORMATION

Corresponding Authors

Daniel R. Gamelin − *Department of Chemistry and Molecular Engineering and Sciences Institute, University of Washington, Seattle, Washington 98195, United States;* orcid.org/0000-0003-2888-9916; Email: gamelin@uw.edu

J. Devin Mackenzie − *Department of Materials Science and Engineering, University of Washington, Seattle, Washington 98195, United States; Department of Mechanical Engineering, University of Washington, Seattle, Washington 98195, United States*; Email: jdmacken@uw.edu

Authors

Theodore A. Cohen − *Molecular Engineering and Sciences Institute, University of Washington, Seattle, Washington 98195, United States;* orcid.org/0000-0001-7170-3211

David Sharp − *Department of Physics, University of Washington, Seattle, Washington 98195, United States;* orcid.org/0000-0002-1034-8567

Kyle T. Kluherz − *Department of Chemistry, University of Washington, Seattle, Washington 98195, United States;* orcid.org/0000-0002-7986-5167

Yueyang Chen − *Department of Electrical and Computer Engineering, University of Washington, Seattle, Washington 98195, United States;* orcid.org/0000-0002-4390-550X

Christopher Munley − *Department of Physics, University of Washington, Seattle, Washington 98195, United States*

Rayne T. Anderson − *Department of Chemistry and Department of Materials Science and Engineering, University of Washington, Seattle, Washington 98195, United States;* orcid.org/0000-0001-8357-0452

Connor J. Swanson − *Department of Materials Science and Engineering, University of Washington, Seattle, Washington 98195, United States*

James J. De Yoreo − *Department of Chemistry and Department of Materials Science and Engineering, University of Washington, Seattle, Washington 98195, United States; Physical Sciences Division, Pacific Northwest National Laboratory, Richland, Washington 99352, United States;* orcid.org/0000-0002-9194-6699

Christine K. Luscombe − *Molecular Engineering and Sciences Institute, Department of Chemistry, and Department of Materials Science and Engineering, University of Washington, Seattle, Washington 98195, United States;* Present Address: pi-Conjugated Polymers Unit, Okinawa Institute of Science and Technology, Onna-son, Okinawa,904−0495, Japan; orcid.org/0000-0001-7456-1343

Arka Majumdar − *Department of Physics, University of Washington, Seattle, Washington 98195, United States; Department of Electrical and Computer Engineering, University of Washington, Seattle, Washington 98195, United States;* orcid.org/0000-0003-0917-590X

Complete contact information is available at: https://pubs.acs.org/10.1021/acs.nanolett.2c00473

https://doi.org/10.1021/acs.nanolett.2c00473
Nano Lett. XXXX, XXX, XXX−XXX

Notes

The authors declare no competing financial interest.

■ ACKNOWLEDGMENTS

This research was primarily supported by the National Science Foundation (NSF) through the UW Molecular Engineering Materials Center, a Materials Research Science and Engineering Center (DMR-1719797 to D.R.G., J.D.M., J.J.D.Y., and C.K.L.). This work was also supported by the State of Washington through the Washington Research Foundation and the Joint Center for Deployment and Research in Earth Abundant Materials (to J.D.M.). Part of this work was conducted at the Washington Clean Energy Testbeds and the Photonic Research Center, facilities operated by the University of Washington Clean Energy Institute. Part of this work was conducted at the Molecular Analysis Facility, a National Nanotechnology Coordinated Infrastructure site at the University of Washington that is supported in part by the National Science Foundation (ECC-1542101), the University of Washington, the Molecular Engineering & Sciences Institute, and the Clean Energy Institute. We gratefully acknowledge the assistance of Kelly Walsh for collecting XRD data and Jacob Kremish-Wells for assistance in preparing printing solutions. We also acknowledge Yunping Huang for helpful discussions.

■ REFERENCES

(1) Thompson, L. F., An Introduction to Lithography. In *Introduction to Microlithography*; American Chemical Society: 1983; Vol. *219*, pp 1−13.

(2) Xia, Y.; Rogers, J. A.; Paul, K. E.; Whitesides, G. M. Unconventional Methods for Fabricating and Patterning Nanostructures. *Chem. Rev.* **1999**, *99*, 1823−1848.

(3) Kash, K.; Scherer, A.; Worlock, J. M.; Craighead, H. G.; Tamargo, M. C. Optical Spectroscopy of Ultrasmall Structures Etched from Quantum Wells. *Appl. Phys. Lett.* **1986**, *49*, 1043−1045.

(4) Senellart, P.; Solomon, G.; White, A. High-Performance Semiconductor Quantum-Dot Single-Photon Sources. *Nat. Nanotechnol.* **2017**, *12*, 1026−1039.

(5) Suh, Y.-H.; Shin, D.-W.; Chun, Y. T. Micro-to-Nanometer Patterning of Solution-Based Materials for Electronics and Optoelectronics. *RSC Adv.* **2019**, *9*, 38085−38104.

(6) Tekin, E.; Smith, P. J.; Hoeppener, S.; van den Berg, A. M. J.; Susha, A. S.; Rogach, A. L.; Feldmann, J.; Schubert, U. S. Inkjet Printing of Luminescent CdTe Nanocrystal−Polymer Composites. *Adv. Funct. Mater.* **2007**, *17*, 23−28.

(7) Wood, V.; Panzer, M. J.; Chen, J.; Bradley, M. S.; Halpert, J. E.; Bawendi, M. G.; Bulović, V. Inkjet-Printed Quantum Dot−Polymer Composites for Full-Color AC-Driven Displays. *Adv. Mater.* **2009**, *21*, 2151−2155.

(8) Lan, L.; Zou, J.; Jiang, C.; Liu, B.; Wang, L.; Peng, J. Inkjet Printing for Electroluminescent Devices: Emissive Materials, Film Formation, and Display Prototypes. *Front. Optoelectron.* **2017**, *10*, 329−352.

(9) Nakao, H.; Murakami, T.; Hirahara, S.; Nagato, H.; Nomura, Y. Head Design for Novel Ink-Jet Printing using Electrostatic Force. *NIP & Digital Fabrication Conference* **1999**, *1999*, 319−322.

(10) Park, J.-U.; Hardy, M.; Kang, S. J.; Barton, K.; Adair, K.; Mukhopadhyay, D. k.; Lee, C. Y.; Strano, M. S.; Alleyne, A. G.; Georgiadis, J. G.; et al. High-Resolution Electrohydrodynamic Jet Printing. *Nat. Mater.* **2007**, *6*, 782−789.

(11) Kim, B. H.; Onses, M. S.; Lim, J. B.; Nam, S.; Oh, N.; Kim, H.; Yu, K. J.; Lee, J. W.; Kim, J.-H.; Kang, S.-K.; et al. High-Resolution Patterns of Quantum Dots Formed by Electrohydrodynamic Jet Printing for Light-Emitting Diodes. *Nano Lett.* **2015**, *15*, 969−973.

(12) Li, H.; Duan, Y.; Shao, Z.; Zhang, G.; Li, H.; Huang, Y.; Yin, Z. High-Resolution Pixelated Light Emitting Diodes Based on Electrohydrodynamic Printing and Coffee-Ring-Free Quantum Dot Film. *Adv. Mater. Technol.* **2020**, *5*, 2000401.

(13) Grotevent, M. J.; Hail, C. U.; Yakunin, S.; Dirin, D. N.; Thodkar, K.; Borin Barin, G.; Guyot-Sionnest, P.; Calame, M.; Poulikakos, D.; Kovalenko, M. V.; et al. Nanoprinted Quantum Dot−Graphene Photodetectors. *Adv. Opt. Mater.* **2019**, *7*, 1900019.

(14) Brossard, F. S. F.; Pecunia, V.; Ramsay, A. J.; Griffiths, J. P.; Hugues, M.; Sirringhaus, H. Inkjet-Printed Nanocavities on a Photonic Crystal Template. *Adv. Mater.* **2017**, *29*, 1704425.

(15) Aellen, M.; Rossinelli, A. A.; Keitel, R. C.; Brechbühler, R.; Antolinez, F. V.; Cui, J.; Norris, D. J. Reconsidering the Design of Planar Plasmonic Lasers: Gain, Gap Layers, and Mode Competition. 2021, 2101.05881. *arXiv[physics]*. https://arxiv.org/abs/2101.05881 (accessed October 22, 2021).

(16) Kress, S. J. P.; Richner, P.; Jayanti, S. V.; Galliker, P.; Kim, D. K.; Poulikakos, D.; Norris, D. J. Near-Field Light Design with Colloidal Quantum Dots for Photonics and Plasmonics. *Nano Lett.* **2014**, *14*, 5827−5833.

(17) Kress, S. J. P.; Cui, J.; Rohner, P.; Kim, D. K.; Antolinez, F. V.; Zaininger, K.-A.; Jayanti, S. V.; Richner, P.; McPeak, K. M.; Poulikakos, D.; Norris, D. J.; et al. A Customizable Class of Colloidal-Quantum-Dot Spasers and Plasmonic Amplifiers. *Sci. Adv.* **2017**, *3*, No. e1700688.

(18) Kress, S. J. P.; Antolinez, F. V.; Richner, P.; Jayanti, S. V.; Kim, D. K.; Prins, F.; Riedinger, A.; Fischer, M. P. C.; Meyer, S.; McPeak, K. M.; et al. Wedge Waveguides and Resonators for Quantum Plasmonics. *Nano Lett.* **2015**, *15*, 6267−6275.

(19) Hail, C. U.; Höller, C.; Matsuzaki, K.; Rohner, P.; Renger, J.; Sandoghdar, V.; Poulikakos, D.; Eghlidi, H. Nanoprinting Organic Molecules at the Quantum Level. *Nat. Commun.* **2019**, *10*, 1880.

(20) Huang, C.-Y.; Zou, C.; Mao, C.; Corp, K. L.; Yao, Y.-C.; Lee, Y.-J.; Schlenker, C. W.; Jen, A. K. Y.; Lin, L. Y. $CsPbBr_3$ Perovskite Quantum Dot Vertical Cavity Lasers with Low Threshold and High Stability. *ACS Photonics* **2017**, *4*, 2281−2289.

(21) He, Z.; Chen, B.; Hua, Y.; Liu, Z.; Wei, Y.; Liu, S.; Hu, A.; Shen, X.; Zhang, Y.; Gao, Y.; et al. CMOS Compatible High-Performance Nanolasing Based on Perovskite−SiN Hybrid Integration. *Adv. Opt. Mater.* **2020**, *8*, 2000453.

(22) Park, Y.-S.; Guo, S.; Makarov, N. S.; Klimov, V. I. Room Temperature Single-Photon Emission from Individual Perovskite Quantum Dots. *ACS Nano* **2015**, *9*, 10386−10393.

(23) Utzat, H.; Sun, W.; Kaplan, A. E. K.; Krieg, F.; Ginterseder, M.; Spokoyny, B.; Klein, N. D.; Shulenberger, K. E.; Perkinson, C. F.; Kovalenko, M. V.; et al. Coherent Single-Photon Emission from Colloidal Lead Halide Perovskite Quantum Dots. *Science* **2019**, *363*, 1068−1072.

(24) Crane, M. J.; Jacoby, L. M.; Cohen, T. A.; Huang, Y.; Luscombe, C. K.; Gamelin, D. R. Coherent Spin Precession and Lifetime-Limited Spin Dephasing in $CsPbBr_3$ Perovskite Nanocrystals. *Nano Lett.* **2020**, *20*, 8626−8633.

(25) Rainò, G.; Becker, M. A.; Bodnarchuk, M. I.; Mahrt, R. F.; Kovalenko, M. V.; Stöferle, T. Superfluorescence from Lead Halide Perovskite Quantum Dot Superlattices. *Nature* **2018**, *563*, 671−675.

(26) Cherniukh, I.; Rainò, G.; Stöferle, T.; Burian, M.; Travesset, A.; Naumenko, D.; Amenitsch, H.; Erni, R.; Mahrt, R. F.; Bodnarchuk, M. I.; et al. Perovskite-Type Superlattices from Lead Halide Perovskite Nanocubes. *Nature* **2021**, *593*, 535−542.

(27) Palazon, F.; Akkerman, Q. A.; Prato, M.; Manna, L. X-ray Lithography on Perovskite Nanocrystals Films: From Patterning with Anion-Exchange Reactions to Enhanced Stability in Air and Water. *ACS Nano* **2016**, *10*, 1224−1230.

(28) Minh, D. N.; Eom, S.; Nguyen, L. A. T.; Kim, J.; Sim, J. H.; Seo, C.; Nam, J.; Lee, S.; Suk, S.; Kim, J.; et al. Perovskite Nanoparticle Composite Films by Size Exclusion Lithography. *Adv. Mater.* **2018**, *30*, 1802555.

(29) Pan, J.-A.; Ondry, J. C.; Talapin, D. V. Direct Optical Lithography of $CsPbX_3$ Nanocrystals *via* Photoinduced Ligand

https://doi.org/10.1021/acs.nanolett.2c00473
Nano Lett. XXXX, XXX, XXX−XXX

Cleavage with Postpatterning Chemical Modification and Electronic Coupling. *Nano Lett.* **2021**, *21*, 7609−7616.
(30) Duan, M.; Feng, Z.; Wu, Y.; Yin, Y.; Hu, Z.; Peng, W.; Li, D.; Chen, S.-j.; Lee, C.-Y.; Lien, A. Inkjet-Printed Micrometer-Thick Patterned Perovskite Quantum Dot Films for Efficient Blue-to-Green Photoconversion. *Adv. Mater. Technol.* **2019**, *4*, 1900779.
(31) Liu, J.; Shabbir, B.; Wang, C.; Wan, T.; Ou, Q.; Yu, P.; Tadich, A.; Jiao, X.; Chu, D.; Qi, D.; et al. Flexible, Printable Soft-X-Ray Detectors Based on All-Inorganic Perovskite Quantum Dots. *Adv. Mater.* **2019**, *31*, 1901644.
(32) Altintas, Y.; Torun, I.; Yazici, A. F.; Beskazak, E.; Erdem, T.; Serdar Onses, M.; Mutlugun, E. Multiplexed Patterning of Cesium Lead Halide Perovskite Nanocrystals by Additive Jet Printing for Efficient White Light Generation. *Chem. Eng. J.* **2020**, *380*, 122493.
(33) Yakunin, S.; Chaaban, J.; Benin, B. M.; Cherniukh, I.; Bernasconi, C.; Landuyt, A.; Shynkarenko, Y.; Bolat, S.; Hofer, C.; Romanyuk, Y. E.; et al. Radiative lifetime-encoded unicolour security tags using perovskite nanocrystals. *Nat. Commun.* **2021**, *12*, 981.
(34) Rainò, G.; Landuyt, A.; Krieg, F.; Bernasconi, C.; Ochsenbein, S. T.; Dirin, D. N.; Bodnarchuk, M. I.; Kovalenko, M. V. Underestimated Effect of a Polymer Matrix on the Light Emission of Single $CsPbBr_3$ Nanocrystals. *Nano Lett.* **2019**, *19*, 3648−3653.
(35) Baranov, D.; Fieramosca, A.; Yang, R. X.; Polimeno, L.; Lerario, G.; Toso, S.; Giansante, C.; Giorgi, M. D.; Tan, L. Z.; Sanvitto, D.; et al. Aging of Self-Assembled Lead Halide Perovskite Nanocrystal Superlattices: Effects on Photoluminescence and Energy Transfer. *ACS Nano* **2021**, *15*, 650−664.
(36) Fong, C. F.; Yin, Y.; Chen, Y.; Rosser, D.; Xing, J.; Majumdar, A.; Xiong, Q. Silicon Nitride Nanobeam Enhanced Emission from All-Inorganic Perovskite Nanocrystals. *Opt. Express, OE* **2019**, *27*, 18673−18682.
(37) Cohen, T. A.; Huang, Y.; Bricker, N. A.; Juhl, C. S.; Milstein, T. J.; MacKenzie, J. D.; Luscombe, C. K.; Gamelin, D. R. Modular Zwitterion-Functionalized Poly(isopropyl methacrylate) Polymers for Hosting Luminescent Lead Halide Perovskite Nanocrystals. *Chem. Mater.* **2021**, *33*, 3779−3790.
(38) Shafrin, E. G.; Zisman, W. A. Constitutive relations in the wetting of low energy surfaces and the theory of the retraction method of preparing monolayers. *J. Phys. Chem.* **1960**, *64*, 519−524.
(39) Klein, T.; Yan, S.; Cui, J.; Magee, J. W.; Kroenlein, K.; Rausch, M. H.; Koller, T. M.; Fröba, A. P. Liquid Viscosity and Surface Tension of n-Hexane, n-Octane, n-Decane, and n-Hexadecane up to 573 K by Surface Light Scattering. *J. Chem. Eng. Data* **2019**, *64*, 4116−4131.
(40) Schlisske, S.; Held, M.; Rödlmeier, T.; Menghi, S.; Fuchs, K.; Ruscello, M.; Morfa, A. J.; Lemmer, U.; Hernandez-Sosa, G. Substrate-Independent Surface Energy Tuning *via* Siloxane Treatment for Printed Electronics. *Langmuir* **2018**, *34*, 5964−5970.
(41) Wang, D. Z.; Jayasinghe, S. N.; Edirisinghe, M. J. High Resolution Print-Patterning of a Nano-Suspension. *J. Nanopart. Res.* **2005**, *7*, 301−306.
(42) Wang, D. Z.; Jayasinghe, S. N.; Edirisinghe, M. J.; Luklinska, Z. B. Coaxial Electrohydrodynamic Direct Writing of Nano-Suspensions. *J. Nanopart. Res.* **2007**, *9*, 825−831.
(43) Rohner, P.; Reiser, A.; Rabouw, F. T.; Sologubenko, A. S.; Norris, D. J.; Spolenak, R.; Poulikakos, D. 3D Electrohydrodynamic Printing and Characterisation of Highly Conductive Gold Nanowalls. *Nanoscale* **2020**, *12*, 20158−20164.
(44) Chen, Y.; Ryou, A.; Friedfeld, M. R.; Fryett, T.; Whitehead, J.; Cossairt, B. M.; Majumdar, A. Deterministic Positioning of Colloidal Quantum Dots on Silicon Nitride Nanobeam Cavities. *Nano Lett.* **2018**, *18*, 6404−6410.
(45) Fryett, T. K.; Chen, Y.; Whitehead, J.; Peycke, Z. M.; Xu, X.; Majumdar, A. Encapsulated Silicon Nitride Nanobeam Cavity for Hybrid Nanophotonics. *ACS Photonics* **2018**, *5*, 2176−2181.
(46) Koc, M. A.; Raja, S. N.; Hanson, L. A.; Nguyen, S. C.; Borys, N. J.; Powers, A. S.; Wu, S.; Takano, K.; Swabeck, J. K.; Olshansky, J. H.; et al. Characterizing Photon Reabsorption in Quantum Dot-Polymer Composites for Use as Displacement Sensors. *ACS Nano* **2017**, *11*, 2075−2084.
(47) Chizhik, A. I.; Gregor, I.; Schleifenbaum, F.; Müller, C. B.; Röling, C.; Meixner, A. J.; Enderlein, J. Electrodynamic Coupling of Electric Dipole Emitters to a Fluctuating Mode Density within a Nanocavity. *Phys. Rev. Lett.* **2012**, *108*, 163002.
(48) Chizhik, A. I.; Gregor, I.; Ernst, B.; Enderlein, J. Nanocavity-Based Determination of Absolute Values of Photoluminescence Quantum Yields. *ChemPhysChem* **2013**, *14*, 505−513.

https://doi.org/10.1021/acs.nanolett.2c00473
Nano Lett. XXXX, XXX, XXX−XXX